

Effect of force during stumbling of the femur fracture with a different ce-mented total hip prosthesis

Zagane Mohammed El Sallah*^{1,2}, Benouis Ali^{2,3} and Sahli Abderahmen²

¹Department of Mechanical Engineering, Faculty of Science Appliqué, University of Tiaret, City Zaaroura, BP 78, Tiaret, Algeria

²Department of Mechanical Engineering, University of Sidi Bel Abbes, LMPM, BP 89, Cité Ben M'hidi, Sidi Bel Abbes 22000, Algeria

³University of Moulay, Tahar Saïda, City Ennasr, BP 138 20000 Saïda, Algeria

(Received June 29, 2018, Revised February 24, 2020, Accepted March 12, 2020)

Abstract. Total hip prosthesis is used for the patients who have hip fracture and are unable to recover naturally. To design highly durable prostheses one has to take into account the natural processes occurring in the bone. Finite element analysis is a computer based numerical analysis method which can be used to calculate the response of a model to a set of well-defined boundary conditions. In this paper, the static load analysis is based, by selecting the peak load during the stumbling activity. Two different implant materials have been selected to study appropriate material. The results showed the difference of maximum von Mises stress and detected the fracture of the femur shaft for different model (Chamley and Osteal) implant with the extended finite element method (XFEM), and after the results of the numerical simulation of XFEM for different was used in determining the stress intensity factors (SIF) to identify the crack behavior implant materials for different crack length. It has been shown that the maximum stress intensity factors were observed in the model of Chamley.

Keywords: totalhip prosthesis (THP); extended finite element method (XFEM); bone fracture; femur; stumbling; stress intensity factor (SIF)

1. Introduction

Total Hip Prosthesis (THP) is an excellent alternative for patients suffering from arthritis or hip fracture (Beswick 2011, Gao 2009). Millions of people undergo total hip replacement every year (Harsha 2013). To avoid injuries and fractures of the femur (cortical bone cement, implant) in patients after the replacement THP, surgeons need published information about the clinical results of different joint replacements; However, many important factors are still very difficult to take into account during these studies. In particular, these aspects related to the patient (skeletal anatomy, bone quality, muscles, level of activity or biological response) or to the surgeon (bone surgery, implant position and fit, joint center relocation or muscle surgery). El'Sheikh *et al.* compared the hip prosthesis component subjected to a dynamic stumbling load and the peak static load of the similar patient load behavior El'Sheikh (2003). Shankaet *et al.* to predict the impact of different material combination pairs on the acetabulum contact model during stumbling cycle to assess the

*Corresponding author, Ph.D., E-mail: salah_cao@yahoo.fr

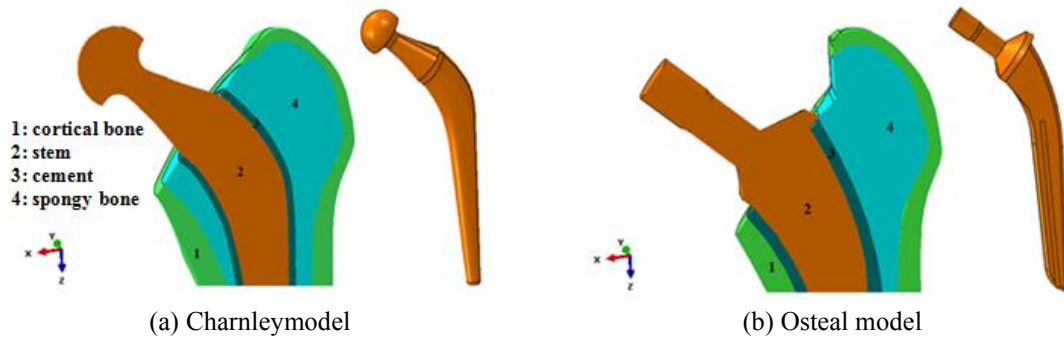


Fig. 1 Three-dimensional femur stems for two models

contact stresses and deformation on the lines of our previous static model (Shankar 2014).

This study aims to evaluate the three dimensional (3D) finite element (FE) inlay retained and only supported partial models were established for use to examine the behavior of the hip total arthroplasty and cracks within the bone cortical with different types of the femoral implant: Charnley stem and the Osteal stem (Fig. 1).

To predict bone femoral fracture models using the techniques is the extended finite element method (XFEM) which enriches the FE approximation space with special functions that introduce the displacement discontinuity across the crack faces and the singular behavior associated with the crack front, and makes its analysis, up to a certain point, independent of the mesh (Moës 1999, Sukumar 2000).

Numerous previous studies have been devoted to analysis of quasi-static mechanical properties and resistance to fracture of the cortical bone tissue have implemented X-FEM For instance, Adel, A. Abdel-Wahab, a two-dimensional numerical (finite-element) fracture model for osteonal bovine cortical bone was developed to account for its microstructure using extended finite element method (X-FEM) (Adel and Abdel-Wahab 2012). Another study, by Bonney *et al.* (2011), was devoted to investigation of local variations in mechanical properties of cortical bone (porcine femur)

In addition, Li *et al.* (2013) to develop a finite-element approach to evaluate the fracture process in cortical bone at micro-scale). For instance, Budyn and Hoc (2007) introduced a multiscale method to simulate multiple crack growth in a cortical bone tissue using X-FEM under simplified tensile loading conditions. In another recent attempt, Liu *et al.* (2010). Developed a homogenised X-FE Mmodel to predict fracture of a proximal femur due to impact

The extended finite element method (XFEM) has emerged as a powerful tool to analyse cracks and measuring SIF Giner (2009). Is an important parameter, which judges whether there is crack propagation. So, the numerical evaluation of the SIF is an important issue in applied fracture mechanics (Bouiadjra 2007). Guian Qian *et al.* (2016) to compare different numerical methods for mode I stress intensity factor (SIF) calculations. Using the finite element method (FEM) and extended finite element method (XFEM). XFEM method shows advantages in modeling cracks, but oscillations in 3D.

After analysis of comparisons of predicted and fracture patterns for different model (Charnley and Osteal) implant under the forces during stumbling and show the von Mises stress distribution on the hip prosthesis total.

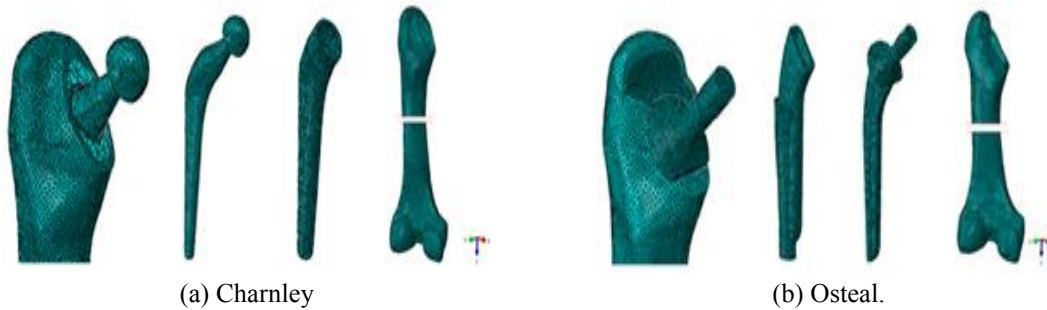


Fig. 2 Finite element meshes of hip prosthesis components

Table 1 Material properties used in FE model

Materials	Young's modulus E (Gpa)	Poisson ratio ν	Yield Strength (Gpa)	Ultimate Tensile Strength (Gpa)	Reference
Charnley stem stainless steel 316 L	230	0.3	0.455	0.65	Bronzino (2000). Kayabasi (2006)
Osteal stem Ti- 6Al4V	110	0.3	0.795	0.86	Pyburn (2004)
Cortical bone	17	0.36	0.16	0.035	Monif (2012)
Bone Cement	2	0.38	0,0438	0.0353	Darwish, (2009), Bergmann (2001)
Cancellous Bone	0.5	0.3	0.00389	-	Darwish (2009), Bergmann (2001)

2. Finite element model

The 3D FE models the femur, cement layer and femoral prosthesis were meshed by four nodes, tetrahedral element (C3D4). The femur, bone cement and Charnley prosthesis were divided into 855 583, 88811, and 229 065 elements, respectively, in the smallest mesh size. The complete Charnley model (stem, bone cement and femur) has in total 1173459 elements. Are shown in Fig. 2(a) and model of Osteal. The femur, cement and the femoral prosthesis were divided into 925 543, 92 851 and 329 065 elements, respectively, The complete Osteal model (stem, bone cement and femur) has in total 1347459 elements. Are shown in Fig. 2(b).

3. Material properties

The mechanical properties of the materials are presented in Table 1. The cortical bone was considered a transversely isotropic elastic material, whereas the spongy bone, cement, Charnley stem stainless steel 316 L, and Osteal stem Ti-6Al4V were considered linear isotropic elastic materials. To assign material properties of the cortical bone, elastic properties were inserted into ABAQUS.

4. Loading condition

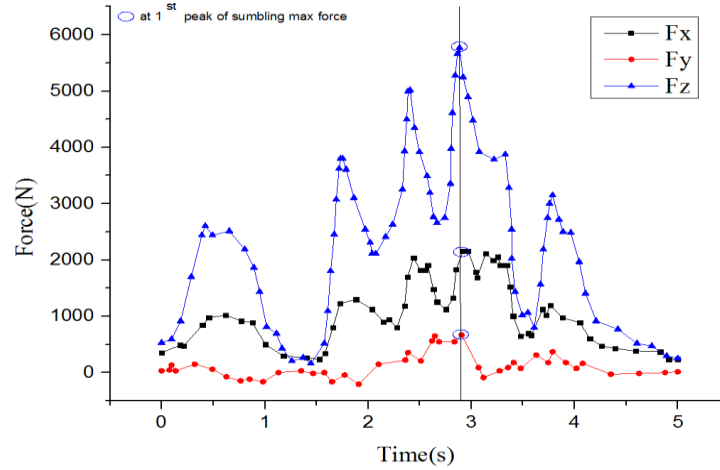


Fig. 3 The variation of forces applied on the prosthesis during stumbling (Bregmann 2001)

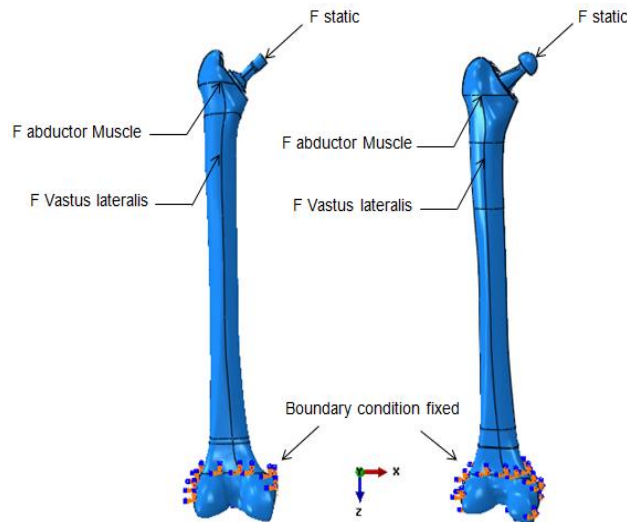


Fig. 4 Boundary conditions and the distribution of the applied and muscle forces on THP

The loading applied was taken from the work of Bergman *et al* (1993) it is illustrated in Fig. 3 which represent loading pattern for stumbling. In static analysis, the maximum force analysis was employed to simulate simplified loading on the implanted femur for stumbling activity, this load analysis is based, by selecting the peak load during the stumbling activity. stumbling resultant force, F , on the head of the femur is 8.7 times the body weight ($BW=70$ kg) at 58% of the gait cycle. This can be resolved into:

$$F_x: -2053.02 \text{ (N)} \quad F_y: 613.77 \text{ (N)} \quad F_z: 5693.49 \text{ (N)}$$

In this study, the magnitudes and the directions of muscle forces data by Bregmann (2001). An abductor muscle load $F_{abductor}$ muscle is applied to the proximal area of the greater trochanter. An iliotibial-tract load $F_{iliotibial}$ tract is applied to the bottom of the femur in the longitudinal femur direction is used. They are shown in (Table 2). The boundary condition was applied by fixing the

Table 2 Muscle load magnitudes applied to the FE model (Bregmann 2001)

Force	F_x (N)	F_y (N)	F_z (N)
Abductor	465.9	34.5	695.0
VastusLateralis	7.2	148.6	746.3

Table 3 Contact details (Ramaniraka 2000)

Femur head- Stem	Cancellous- Cortical	PMMA-Cancellous	Femur head-XLPE	Stem-PMMA
Bonded		Frictional contact ($\mu=1$)	Frictional contact ($\mu=0.2$)	Frictional contact ($\mu=0.4$)

distal epiphysis, which is the distal end of the femur that is connected to the knee (Behrens *et al.* 2009).

Fig. 4 shows the coordinate system used to represent the direction of the forces components.

Optimum values of coefficient of friction, 0.4 for cement-stem and 1.0 for cement-bone interfaces, were considered respectively (Ramaniraka 2000).

5. Fracture criteria for X-FEM

The X-FEM was first introduced by Belytschko and Blackand, and then, it was employed by many researches to carry out their study in the field of fracture mechanics (Abdelaziz 2008). Extended finite element method (X-FEM) is the most effective numerical method to solve discrete mechanical problem. The XFEM was applied to simulate crack initiation and propagation of the model, the basis for damage initiation as per the criterion of the maximum principal stress (σ_1) as indicated in Eq. (1)

$$f^e = \frac{\sigma_1^e}{\langle \sigma_{\max}^* \rangle} \quad (1)$$

The symbol $\langle \rangle$ represents the Macaulay bracket with the usual interpretation that is:

$$\begin{aligned} \langle \sigma_{\max}^* \rangle &= 0 \text{ if } \sigma_1 < 0 \\ \text{And } \langle \sigma_{\max}^* \rangle &= \sigma_1 \text{ if } \sigma_1 \geq 0 \end{aligned}$$

Compressive stress does not initiate the damage. When the boot $f^e \geq 0$ criteria is met. Developed in commercial finite-element software-Abaqus (Dassault Systèmes 2013). The parameters required by the X-FEM for models were selected on the basis of experimental data from the literature Table 4. Mischinski (2013).

5.1 Calculation of the stress intensity factor by XFEM

XFEM was mainly developed to compute discontinuous and singular problems and it also simplifies the modeling of cracked structures and components. Therefore, XFEM can also be used for calculating SIF. The advantage of XFEM lies in the crack modeling, because no remeshing is needed in the crack growth problems and the crack path can be calculated. Discontinuities can also be within elements. The essential idea of XFEM is to use a displacement field approximation that

Table 4 X-FEM damage parameters(Susan Mischinski 2013).

Boneproperties		
σ_{nc} (Mpa)	G_{nc} (N/mm)	G_{sc} (N/mm)
116	1.16	2.97

σ_{nc} : the normal strength; G_{nc} : fracture toughness for opening mode; G_{sc} : shear mode

can model any crack face discontinuity and the near crack-tip asymptotic stress field. As a consequence, it is not necessary to modify the mesh to consider a specific crack; at most, moderate refinement must be introduced around the crack to achieve good accuracy (Moës 1999, Sukumar 2000). Furthermore, XFEM has been implemented in the commercial FE code ABAQUS 2013.

The displacement approximation for the extended finite element formulation used for crack modeling takes the form

$$U_{XFEM}(X) = \sum_{i \in I} Ni(X)H(X)ai + \sum_{i \in K} [Ni(X) \sum_{\alpha=1}^4 Fa(X)bia\alpha] \quad (2)$$

Where I is the set of all nodes in the mesh, $Ni(X)$ are the nodal shape function and we are the standard DOFs of node i (ui represents the physical nodal displacement for non-enriched nodes only). The subsets J and K contain the nodes enriched with the Generalized Heaviside function $H(X)$ or the crack-tip. Functions $F\alpha(X)$, respectively, and $ai, b_{i\alpha}$ are the corresponding DOFs. Fig. 5 shows the enrichment method in XFEM. The nodal degrees of freedom corresponding to the displacement are $iu, j a, k b\alpha, Ni, Nj, Nk$ are the shape functions respectively. $H(x)$ is the generalized Heaviside function which takes the value +1 if x is above the crack and -1 otherwise.

$$H(x) = \begin{cases} +1 & \text{above the crack} \\ -1 & \text{below the crack} \end{cases} \quad (3)$$

$x \alpha \varphi$ is the asymptotic crack-tip fields, which implies the discontinuity occurs at the location of the crack.

$$b_k^a = \left(\sqrt{r} \sin \frac{\theta}{2}, \sqrt{r} \cos \frac{\theta}{2}, \sqrt{r} \sin \theta \sin \frac{\theta}{2}, \sqrt{r} \sin \theta \cos \frac{\theta}{2} \right) \quad (4)$$

Where (r, θ) is the local polar coordinates at the crack tip. Note that the first function in Eq. (4) is discontinuous across the crack faces where the last three functions are continuous.

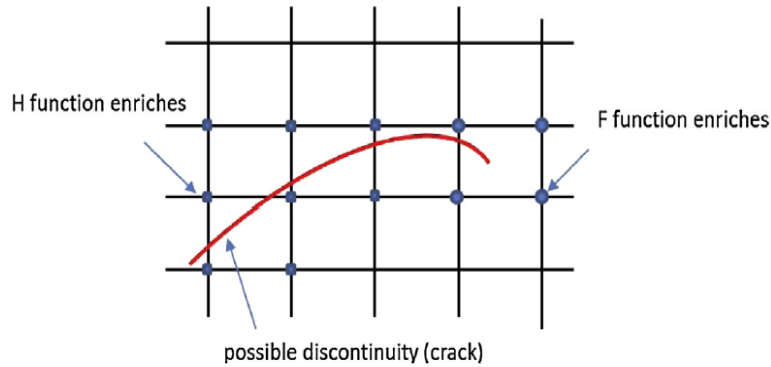


Fig. 5 Enrichment method in XFEM

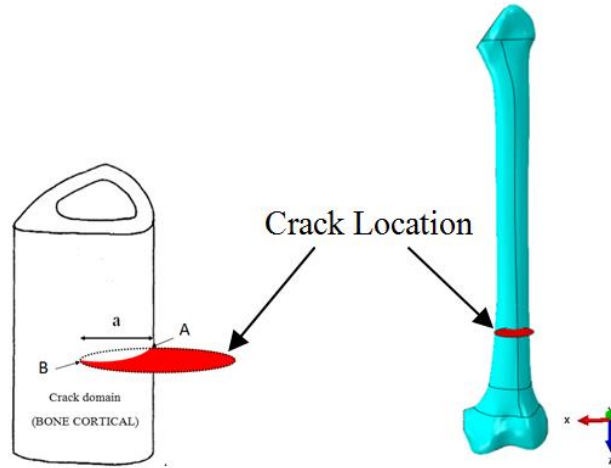


Fig. 6 Defining a crack for X-FEM

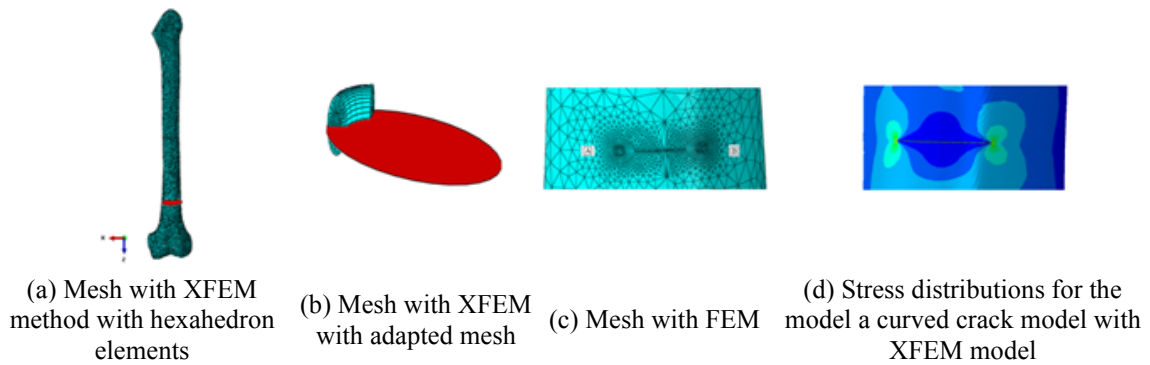


Fig. 7 Meshes for model with curved crack

To calculate the stress intensity factors (SIF) to identify the crack behavior implant materials for different crack length (2, 10 and 30 mm). The crack is located at the diaphysis femoral and its radius is defined in Fig. 6.

The main advantage of the X-FEM besides the accuracy in predicting the crack growth path and fracture parameters is omission of special meshing for crack models in numerical analysis (Waisman 2010, Wyart 2008). The X-FEM mesh, as shown in Fig. 7(a), is built with a regular linear hexahedrons 3D grid. A mesh adapted to the crack geometry can be used to minimize the calculation error in the XFEM study. Fig. 7(b) shows the mesh, adapted to the crack geometry.

6. Results and discussions

The stresses may occur as tensile, compressive, shear, or a stress combination known as equivalent Von Mises stresses. Von Mises stresses depend on the entire stress field and are a widely used indicator of the possibility of damage occurrence. Thus, Von Mises stress was chosen for presentation of results. The stress distribution was identified for each component of the hip

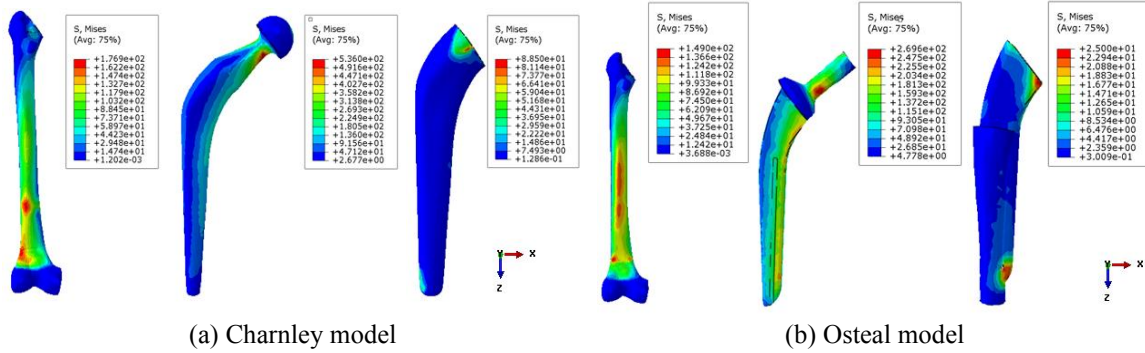


Fig. 8 Von Mises stresses in the hip prostheses components: stem, cement and femur bone

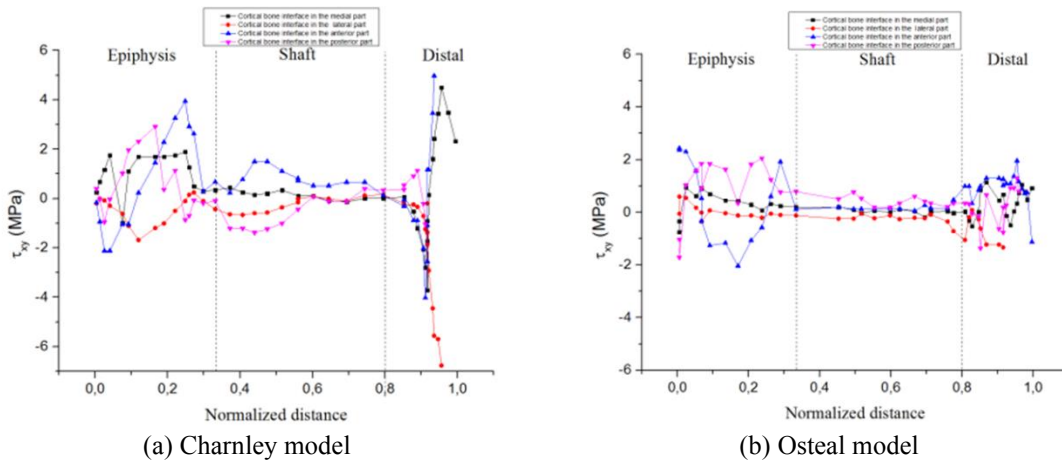


Fig. 9 Shear stresses along the different regions of the bone cortical

prosthesis for Charnley and Osteal models. The values obtained of these stresses around the components of the prostheses are shown in Fig. 8.

Comparing the stress distribution on the hip prostheses, it can be observed the stress concentration will be always at the neck area. Again, this is reasonable since there is a cross section transition at the neck area that it should always exhibit high stress. The maximum tensile stress being located in the middle of the lateral side of the prosthesis stem with a peak stresses almost equal (536 MPa for Charnley model and 269.6 MPa for Osteal model), for the comparison of stress distribution in the cement mantle The maximum stress is below 88.5 MPa for Charnley model and 25 MPa for Osteal model, in spite of the fact that the peak tensile stress for the Charnley model is greater than that of Osteal model one, it was localized in a small region in the inner interior side of the upper proximal part. For the femurs of the two models the maximum tensile stress exists in the distal part with a value of 176.9 MPa which is greater than that for the Osteal model of 149 MPa. By using the static analysis the treated femur expected to bend in the medial side showed resistance to the vertical applied load. As a result, the peak tensile stress is localized in the upper third of the lateral side, Fig. 7.

Fig. 9 show the variation of the shear stresses along the different regions of the cortical bone of the Charnley and Osteal prostheses. For Charnley prosthesis, the high value of shear stress in the

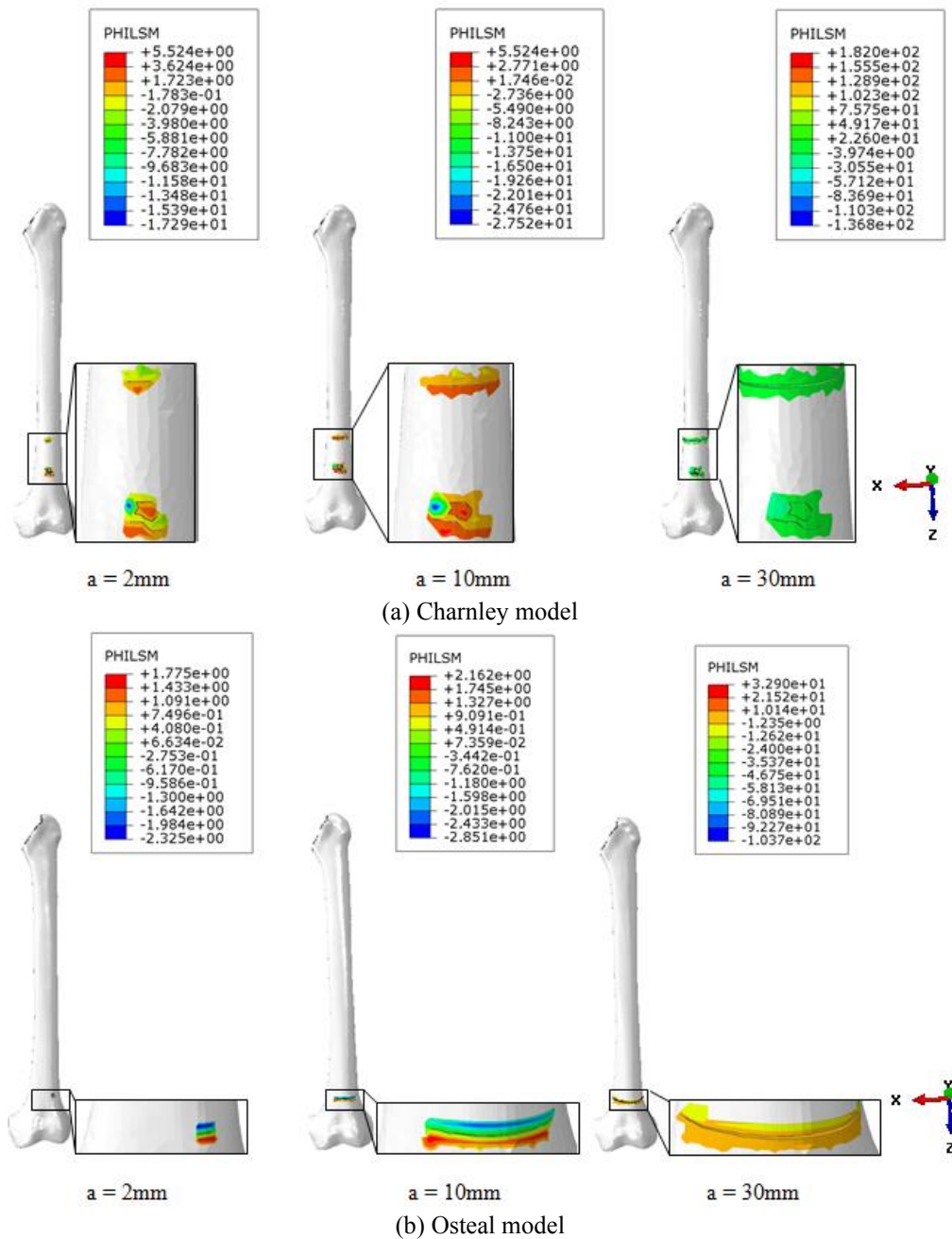


Fig. 10 X-FEM fractures patterns for the different prosthesis in the bone femoral

cement mantle is observed at cortical bone interface, the maximum stress value is about 5 MPa. For Osteal prosthesis, the maximum value of shear stress (2.5 MPa) is localized in the epiphysis region at cortical bone.

The Fig. 10 shows the simulation results with the X-FEM we detected the crack initiation and

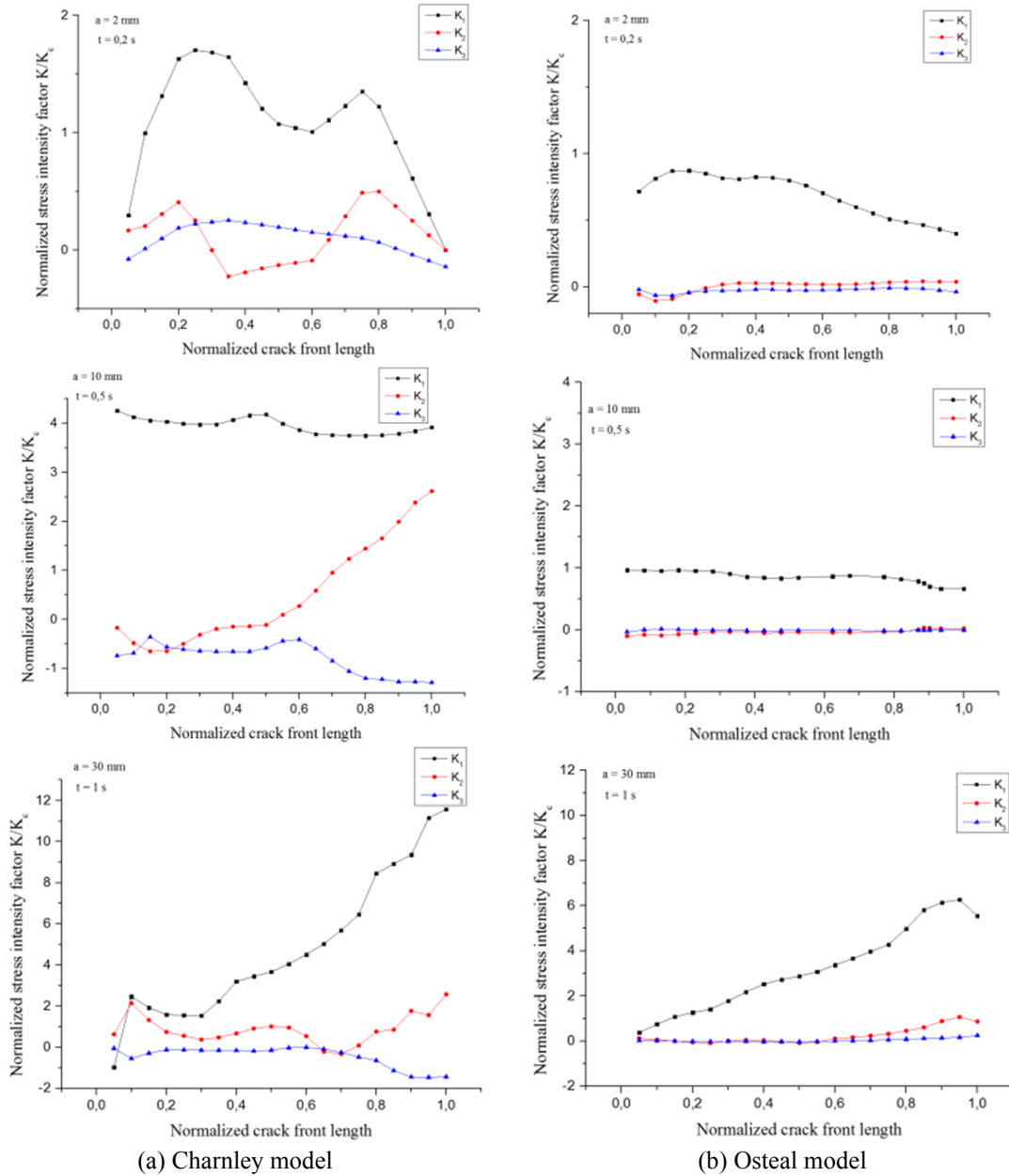


Fig. 11 stress intensity factor of two implanted

follow its propagation in the femur, the fractures propagate through the femoral shaft in its lower part flow third horizontal path in the shaft section for the two models (Charnley and Osteal implant) and resulting from the complete rupture of the shaft femur.

Fig. 11 shows the stress intensity factors (K_I , K_{II} , K_{III}) as a function of the normalized distance of the crack forehead (contour) and has a length (2, 10 and 30 mm). The results of SIFs were taken at mode I. Because the SIFs at mode II and mode III were very small compared with at the value of

modes I, the mode II and mode III values were not taken into account.

In the model Osteal, the KI for the cracks in the different length, regardless, in the lateral to the medial part, the initiation of the crack propagates from the point (A) to point (B), started from a maximum value and gradually decreased to a minimum value, to the length of 10mm beyond this length this phenomenon is reversed. Same observation for model Charnley with significant values compared to the Osteal. That is to say, which means that the latter absorbs the load exerted by the patient.

7. Conclusions

In this paper, three selected methods (stress distribution, crack with X-FEM, stress intensity factor) are applied to compare of model Charnley and Osteal.

From the results, it can be concluded that:

(1) The difference of stress distributions in models The stress values in the bone femur are affected by the material, design and shape of the femoral stem.

In addition, the critical region is still predicted to be in the neck region (proximal part) for both hip prostheses with Charnley and Osteal stems.

(2) X-FEM shows advantages in modeling crack and provides reasonable results. To simulate cracking initiation and propagation was demonstrated to be effective for fracture analysis of bone.the well-known Charnley model. The Osteal prosthesis can have the longest life span X-FEM is recommended in modeling complicated cracks and structures.

(3) The KI values along the crack front showed oscillations, which may be due to the limitation of the enrichmentfunction and limitations of the energy release integral implementation and the extraction domains. Mode I was the most dominant mode of loading crack in the bone cortical.

After a comparison between the present results of the two models confirm that the Osteal model of the hip prosthesis gives weak shear stresses in the bone cortical compared to the well-known Charnley model. The Osteal prosthesis can have the longest life span.

Reference

- ABAQUS/Standard Version 6.13-1 (2013), Analysis User's Manual, Dassault Systèmes Simulia Corporation, Providence, RI, Hibbitt, Karlsson, Sorensen, Abaqus 6.13.1 Manual.
- Abdel-Wahab, A.A., Maligno, A.R. and Silberschmidt, V.V. (2012), "Micro-scale modelling of bovine cortical bone fracture: Analysis of crack propagation and microstructure using X-FEM", *Comput. Mater. Sci.*, **52**, 128-135. <https://doi.org/10.1016/j.commatsci.2011.01.021>.
- Abdelaziz, Y. and Hamouine, A. (2008), "A survey of the extended finite element", *Comput. Struct.*, **86**, 1141-1151. <https://doi.org/10.1016/j.compstruc.2007.11.001>.
- Behrens, B.A., Nolte, I., Wefstaedt, P., Stukenborg-Colsman, C. and Bouguecha, A. (2009), "Numerical investigations on the strain-adaptive bone remodelling in the periprosthetic femur: influence of the boundary conditions", *Biomed. Eng. Online*, **8**(1), 7. <https://doi.org/10.1186/1475-925X-8-7>.
- Bergmann, G. (2001), "HIP98", Free University, BerLin.
- Bergmann, G., Graichen, F. and Rohlmann, A. (1993), "Hip joint forces during walking and running, measured in two patients", *J. Biomech.*, **26**, 969-990. [https://doi.org/10.1016/0021-9290\(93\)90058-M](https://doi.org/10.1016/0021-9290(93)90058-M).
- Beswick, A. and Blom, A.W. (2011), "Bone graft substitutes in hip revision surgery: a comprehensive overview", *Injury*, **42**, S40-S46. <https://doi.org/10.1016/j.injury.2011.06.009>.

- Bonney, H., Colston, B.J. and Goodman, A.M. (2011), "Regional variation in the mechanical properties of cortical bone from the porcine femur", *Med. Eng. Phys.*, **33**(4), 513-520. <https://doi.org/10.1016/j.medengphy.2010.12.002>.
- Bouiadjra, B.B., Belarbi, A., Benbarek, S., Achour, T. and Serier, B. (2007), "FE analysis of the behaviour of microcracks in the cement mantle of reconstructed acetabulum in the total hip prosthesis", *Comput. Mater. Sci.*, **40**, 485-491. <https://doi.org/10.1016/j.commat.2007.02.006>.
- Bronzino, J.D. (2000), *The Biomedical Engineering Handbook*, Volume 1, CRC Press.
- Budyn, É. and Hoc, T. (2007), "Multiple scale modeling for cortical bone fracture in tension using X-FEM", *Eur. J. Comput. Mech./Revue Européenne de Mécanique Numérique*, **16**(2), 213-236. <https://doi.org/10.3166/remn.16.213-236>.
- Darwish, S.M. and Al-Samhan, A.M. (2009), "Optimization of artificial hip joint parameters", *Materialwissenschaft und Werkstofftechnik: Entwicklung, Fertigung, Prüfung, Eigenschaften und Anwendungen technischer Werkstoffe*, **40**(3), 218-223. <https://doi.org/10.1002/mawe.200900430>.
- El'Sheikh, H.F., MacDonald, B.J. and Hashmi, M.S.J. (2003), "Finite element simulation of the hip joint during stumbling: A comparison between static and dynamic loading", *J. Mater. Proc. Technol.*, **43**, 249-255. [https://doi.org/10.1016/S0924-0136\(03\)00352-2](https://doi.org/10.1016/S0924-0136(03)00352-2).
- Gao, L., Wang, F., Yang, P. and Jin, Z. (2009), "Effect of 3D physiological loading and motion on elastohydrodynamic lubrication of metal-on-metal total hip replacements", *Med. Eng. Phys.*, **31**, 720-729. <https://doi.org/10.1016/j.medengphy.2009.02.002>.
- Giner, E., Sukumar, N., Tarancón, J.E. and Fuenmayor, F.J. (2009), "An Abaqus implementation of the extended finite element method", *Eng. Fract. Mech.*, **76**, 347-368. <https://doi.org/10.1016/j.engfracmech.2008.10.015>.
- Harsha, A.P. and Joyce, T.J. (2013), "Comparative wear tests of ultra-high molecular weight polyethylene and cross-linked polyethylene", *J. Eng. Med.*, **227**(5), 600-608. <https://doi.org/10.1177/0954411913479528>.
- Kayabasi, O. and Erzincanli, F. (2006), "Finite element modelling and analysis of a new cemented hip prosthesis", *Adv. Eng. Softw.*, **37**(7), 477-483. <https://doi.org/10.1016/j.advengsoft.2005.09.003>.
- Li, S., Abdel-Wahab, A., Demirci, E. and Silberschmidt, V.V. (2014), "Fracture process in cortical bone: X-FEM analysis of microstructured models", *Fracture Phenomena in Nature and Technology*, Springer, Cham. https://doi.org/10.1007/978-3-319-04397-5_5.
- Liu, X.C., Qin, X. and Du, Z. (2010), "Bone fracture analysis using the extended finite element method (XFEM) with abaqus", *The 34th Annual Meeting of the American Society of Biomechanics*, Brown University.
- Mischinski, S. and Ural, A. (2013), "Interaction of microstructure and microcrack growth in cortical bone: a finite element study", *Comput. Meth. Biomech. Biomed. Eng.*, **16**(1), 81-94. <https://doi.org/10.1080/10255842.2011.607444>.
- Moës, N., Dolbow, J. and Belytschko, T. (1999), "A finite element method for crack growth without remeshing", *Int. J. Numer. Meth. Eng.*, **46**, 131-150. [https://doi.org/10.1002/\(SICI\)1097-0207\(19990910\)46:1<131::AID-NME726>3.0.CO;2-J](https://doi.org/10.1002/(SICI)1097-0207(19990910)46:1<131::AID-NME726>3.0.CO;2-J).
- Monif, M.M. (2012), "Finite element study on the predicted equivalent stresses in the artificial hip joint", *J. Biomed. Sci. Eng.*, **5**, 43-51. <https://doi.org/10.4236/jbise.2012.52007>.
- Pyburn, E. and Goswami, T. (2004), "Finite element analysis of femoral components paper III - hip joints", *Mater. Des.*, **25**(8), 705-713. <https://doi.org/10.1016/j.matdes.2004.01.009>.
- Qian, G., González-Albuixech, V. F., Niffenegger, M. and Giner, E. (2016), "Comparison of KI calculation methods", *Eng. Fract. Mech.*, **156**, 52-67. <https://doi.org/10.1016/j.engfracmech.2016.02.014>.
- Ramaniraka, N.A., Rakotomanana, L.R. and Leyvraz, P.F. (2000), "The fixation of cemented femoral component", *J. Bone Joint Surgery (Br)*, **82**, 297-303.
- Shankar, S. and Manikandan, M. (2014), "Mankandan dynamic contact analysis of total hip prosthesis during stumbling cycle", *J. Mech. Med. Biol.*, **14**(3), 1450041. <https://doi.org/10.1142/S0219519414500419>.
- Sukumar, N., Moës, N., Moran, N. and Belytschko, T. (2000), "Extended finite element method for three-dimensional crack modelling", *Int. J. Numer. Meth. Eng.*, **48**, 1549-1570. [https://doi.org/10.1002/1097-0207\(20000820\)48:11<1549::AID-NME955>3.0.CO;2-A](https://doi.org/10.1002/1097-0207(20000820)48:11<1549::AID-NME955>3.0.CO;2-A).

- Waisman, H. (2010), "An analytical stiffness derivative extended finite element technique for extraction of crack tip Strain Energy Release Rates", *Eng. Fract. Mech.*, **77**, 3204-3215. <https://doi.org/10.1016/j.engfracmech.2010.08.015>.
- Wyart, E., Duflot, M., Coulon, D., Martiny, P., Pardoën, T., Remacle, J.F. and Lani, F. (2008), "Substructuring FE-XFE approaches applied to three-dimensional crack propagation", *J. Comput. Appl. Math.*, **215**, 626-638. <https://doi.org/10.1016/j.cam.2006.03.066>.

CC